Hindawi Publishing Corporation
Advances in Meteorology
Volume 2015, Article ID 383614, 9 pages
http://dx.doi.org/10.1155/2015/383614

Research Article

Temperature Variability over the Po Valley, Italy, according to Radiosounding Data

Boyan Hristozov Petkov

Institute of Atmospheric Sciences and Climate (ISAC), Italian National Research Council (CNR), Via Gobetti 101, 40129 Bologna, Italy

Correspondence should be addressed to Boyan Hristozov Petkov; b.petkov@isac.cnr.it

Received 18 November 2014; Accepted 27 January 2015

Academic Editor: Sven-Erik Gryning

Temperature variations registered above the southeast part of the Po Valley, Italy, have been examined by applying the principal component analysis of radiosounding profiles recorded during the period from 1987 to 2010. Two datasets, considered to describe intra- and interannual oscillations, respectively, were extracted from the measurements data and the results show that both types of fluctuations can be projected onto four empirical orthogonal functions (EOFs), interpreted as vertical distributions of oscillation amplitudes and four uncorrelated time series that represent the evolution of corresponding EOFs. It was found that intra-annual oscillations composed of periods between 30 and 120 days, together with interannual variations of 1- to 7-year period contribute to the highest extent (about 70%) of the temperature oscillations up to 20 km, changing in both cases the phase in the tropopause region. The other three EOFs indicate prevailing weight of the oscillations in the upper troposphere-low stratosphere region and are characterised by longer periods in both types of fluctuations. The intra-annual variations can be accounted for an interaction between Madden-Julian and Arctic oscillations, while the spectral features of interannual fluctuations could be associated with those of Quasi Biennial, El Niño, and North Atlantic global oscillations.

1. Introduction

The air temperature at different altitude levels is strongly affected by dynamical processes and, as a result, it is a subject of variations pertaining to large frequency diapason [1–3]. Such variations could be associated with the numerous patterns of oscillations observed in various atmospheric and oceanic parameters, like Madden-Julian oscillations (MJO) [4, 5], arctic oscillations (AO) [6, 7], quasi-biennial oscillations (QBO) [8], El Niño Southern oscillations (ENSO) [9–11], and North Atlantic oscillations (NAO) [10, 12]. Despite the fact that the major part of these variations is generated in the equatorial and tropical zones on the one hand and in Arctic on the other, they can expand to the midlatitude regions as well. For instance, it was found that ENSO episodes, which are attributed to changes of the sea surface temperature in the tropical Pacific, strongly affect extratropical atmosphere [13] and such propagation is more effective at middle latitudes in the Northern Hemisphere, where ENSO wave-like anomalies are observed up to 35–40 km altitude [11]. The above listed atmospheric oscillations consist of periods occupying comparatively large time scale starting from intraseasonal MJO that are characterised by periods between 40 and 50 days [4] and AO, presenting a very broad time spectrum composed of weekly to seasonal and longer components [14]. Further, QBO is a mode with variable period averaging approximately 28 months [8] and ENSO and NAO oscillations consisted of periods ranging from 2 to 10 years with peaks at 3 and 7 years for ENSO [10] and 2.5 and 6–10 years for NAO [12]. In addition, the interaction among these oscillations or between one of them with the annual cycle could produce amplitude modulations or variations with intermediate frequencies [8, 14–16].

Temperature is the parameter determining the meteorological conditions in the atmosphere and first of all in the troposphere that directly impacts the human life and activity. On the other hand, the temperature governs the phase transformations of the water in the atmosphere and strongly affects the chemical reactions that take place mostly in the middle and upper layers. Hence, the information about temperature

variations over large temporal and spatial scales, yielded from routinely observations, has a primary importance, since the studding of such variations is closely related to the testing and improvement of climatic models [17–20]. The present study is aimed to examine the altitude-temporal features of temperature variations observed over the southeast part of the Po Valley, Italy, by analysing the radiosounding data taken for about 22 years. Such an inquiry tries to characterise the local temperature variability and to link it with the global atmospheric oscillations.

2. Methodology and Data

This section shortly describes the basis of the method adopted to elaborate the radiosounding data in the present analysis and the preliminary processing of the data aiming to create a proper input for the computation procedure.

2.1. Method. The principle component analysis is a powerful tool for examining the spatiotemporal variability of a scalar field presented by a physical variable [21–23]. The method requires the creation of the anomaly data matrix $\mathbf{F}$ or the matrix containing the deviations ΔV from the average trend of the variable V. The spatial distributions of the anomalies ΔV over a grid of n observational points at certain time are presented as rows in $\mathbf{F}$, while the time series composed by m measurements made at uniquely sampled times at corresponding grid points are given as columns:

$$\mathbf{F} = \begin{pmatrix} \Delta V^{\text{at time } t_1}_{\text{at point 1}} & \Delta V^{\text{at time } t_1}_{\text{at point 2}} & \cdots & \Delta V^{\text{at time } t_1}_{\text{at point } n} \\ \Delta V^{\text{at time } t_2}_{\text{at point 1}} & \Delta V^{\text{at time } t_2}_{\text{at point 2}} & \cdots & \Delta V^{\text{at time } t_2}_{\text{at point } n} \\ \vdots & \vdots & \cdots & \vdots \\ \Delta V^{\text{at time } t_m}_{\text{at point 1}} & \Delta V^{\text{at time } t_m}_{\text{at point 2}} & \cdots & \Delta V^{\text{at time } t_m}_{\text{at point } n} \end{pmatrix}. \quad (1)$$

The anomalies ΔV_{ij} $(i = 1, 2, \ldots, m; j = 1, 2, \ldots, n)$ are usually calculated by removing the trend $\overline{\mathbf{V}}_j$ from each column $\mathbf{V}_j$ of the matrix $\mathbf{F}'$, constructed similarly to $\mathbf{F}$ but containing the measurement data V instead of ΔV. The further step is to find the $n \times n$ covariance matrix $\mathbf{C} = [1/(m-1)]\mathbf{F}^T\mathbf{F}$ ($\mathbf{F}^T$ is the transposed matrix $\mathbf{F}$), which can be presented by solving the eigenvalue problem as

$$\mathbf{C}\mathbf{e}_j = \lambda_j \mathbf{e}_j, \quad (2)$$

where $\mathbf{e}_j$ $(j = 1, 2, \ldots, n)$ are the eigenvectors of $\mathbf{C}$ and $\lambda_1 \geq \lambda_2 \geq \cdots \geq \lambda_n \geq 0$ are the corresponding eigenvalues. Since the eigenvectors are orthogonal to each other and result from field measurements data, they are named empirical orthogonal functions (EOF) and describe the spatial distribution of anomaly amplitude. Each of the values

$$w_j = \frac{\lambda_j}{\sum_j \lambda_j} 100\,(\%) \quad (3)$$

represents the weight of the eigenvector $\mathbf{e}_j$ or the contribution of EOF_j to the spatial distribution of ΔV. In practice, only a few of EOFs have significant weight w_j and hence, the decomposition performed through (2) projects the variations presented by n vectors in $\mathbf{C}$ onto a space determined by p orthogonal vectors ($p \ll n$). The cumulative weight $W_p = \sum_{j=1}^{p} w_j$ determined as the sum of the first p values of w_j in the most of the real cases rapidly increases to 100% (see Figure 3) and p can be determined as the value of j for which W_p becomes reasonably close to 100%.

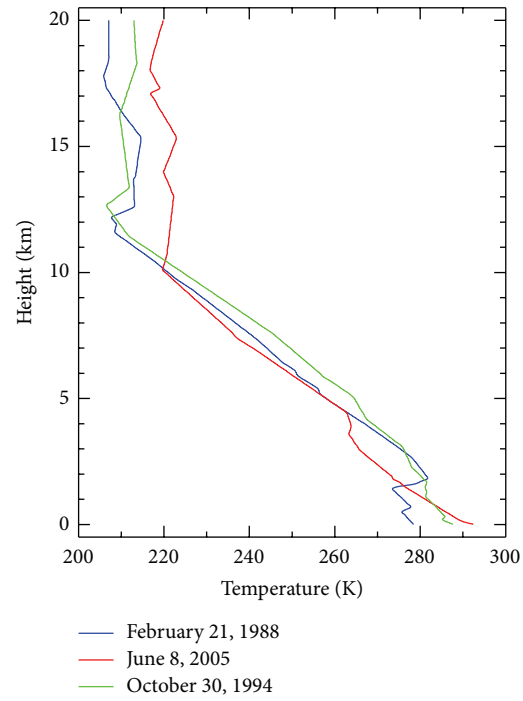

Figure 1: Three temperature profiles recorded at the San Pietro Capofiume station on different days indicated in the graph.

The projection of the anomaly matrix $\mathbf{F}$ onto jth EOF

$$\mathbf{p}_j = \mathbf{F}\mathbf{e}_j \quad (4)$$

is a vector named as the principal component (PC) of the corresponding EOF ($\mathbf{e}_j$) and characterizes the temporal EOF variations.

For the purposes of the present study, $\mathbf{F}$ is structured so that each profile of temperature anomaly $\Delta T_{ij} = \Delta T_{t_i}(z_j)$ found for z_j $(j = 1, 2, \ldots, n)$ height levels provided by a radio sound launched at time t_i $(i = 1, 2, \ldots, m)$ is a row of the matrix:

$$\mathbf{F} = \begin{pmatrix} \Delta T_{11} & \Delta T_{12} & \cdots & \Delta T_{1n} \\ \Delta T_{21} & \Delta T_{22} & \cdots & \Delta T_{2n} \\ \vdots & \vdots & \cdots & \vdots \\ \Delta T_{m1} & \Delta T_{m2} & \cdots & \Delta T_{mn} \end{pmatrix}. \quad (5)$$

Thus, each column is a time series characterising the temperature anomalies at certain altitude level. In the further analysis, the EOFs and PCs have been found by means of the singular value decomposition of the anomaly matrix $\mathbf{F}$ in

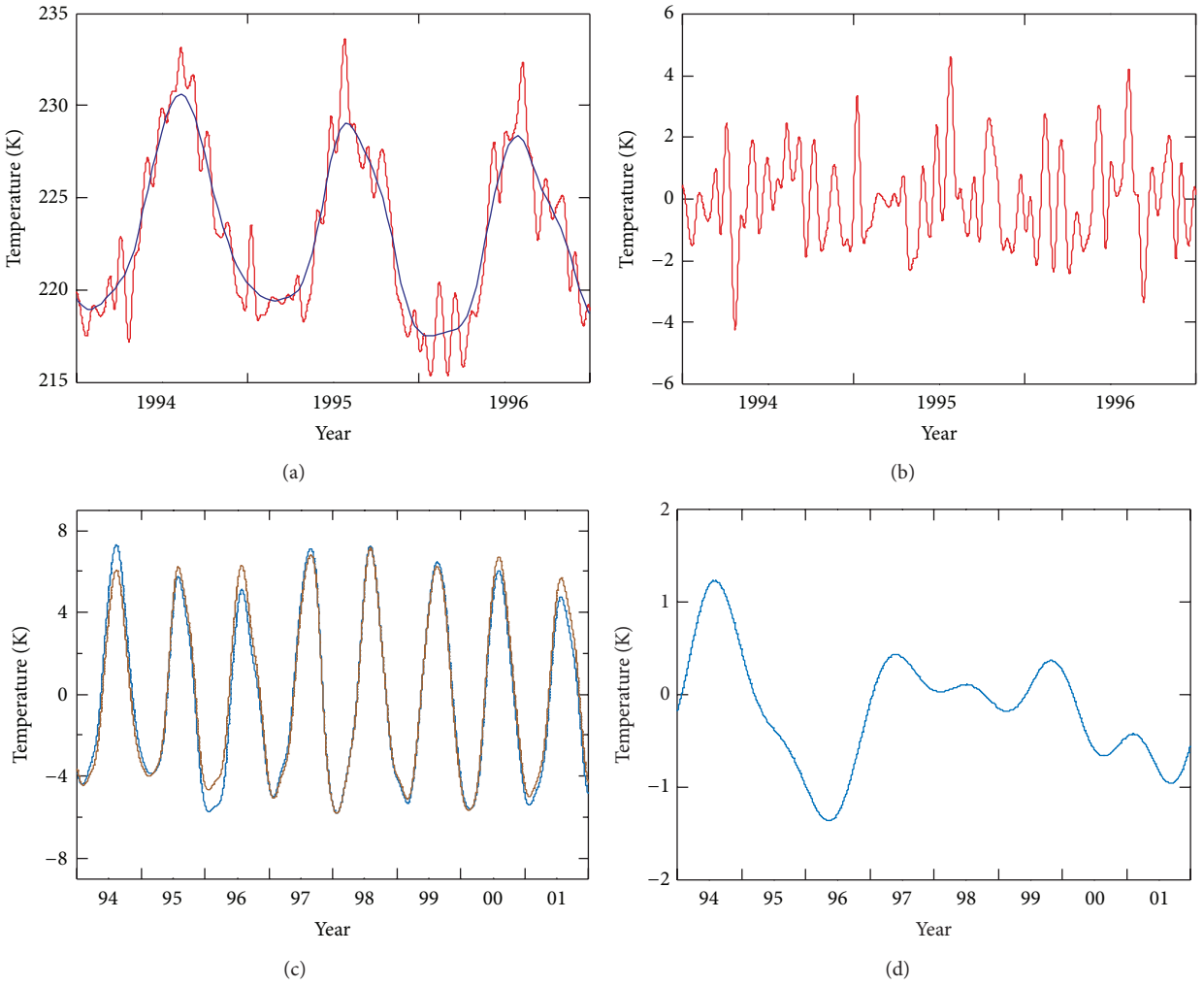

FIGURE 2: Illustration of the preliminary data processing as applied to the data at 10 km altitude. Panel (a) presents the 10-day averaged temperature data (red curve) and the corresponding long-period march (blue curve), while the difference between two curves that is considered to represent the intra-annual variations is given in panel (b). Panel (c) shows detrended long-period variations presented by the azure curve and the oscillations, composed of lower than 1-year cycles (brown curve). The difference between them, given in panel (d), can be associated with the interannual variations.

(5) that is an alternative method presenting **F** as a product of three matrices:

$$\mathbf{F} = \mathbf{PSE}^T, \tag{6}$$

where PCs are the columns of the $m \times r$ matrix **P** and EOFs are the columns of the $r \times n$ matrix **E** [21, 22], where r is the rank of **F**, $r \leq \min(m, n)$, and $r = n$ in our case. The diagonal matrix $\mathbf{S} = (s_{kk} : s_{11} \geq s_{22} \geq \cdots \geq s_{rr} \geq 0)$ contains the singular values, which are connected with the eigenvalues of the covariance matrix **C** as $s_{kk} = \sqrt{\lambda_k}$. In addition, each EOF was multiplied by the associated singular value and each PC was divided by the same value, respectively, that, according to Camp et al. [23], returns the EOFs in dimensional units, Kelvin in our case. The singular value decomposition of the anomaly matrix **F** given by (5) was performed by using the corresponding MATLAB function and the spectral analysis of the PC components was made through the Lomb-Scargle [24, 25] periodogram approach.

2.2. Dataset and Preliminary Elaboration. The present study analyses the data provided by Vaisala radio sounds routinely launched at San Pietro Capofiume station (44°39′N, 11°36′E, 11 m amsl), located in the southeast part of the Po Valley, Italy, twice a day from August 1987 to March 2010. The radio sound gives the vertical distributions of the atmospheric pressure, temperature, relative humidity, and velocity and direction of the wind. Two types of radio sounds were used at the station: Vaisala RS80, until mid-September 2005 and RS92 after that, which are characterised by accuracy of the temperature measurements of ±0.2 and ±0.5 K, respectively [26]. The temperature sensor of RS80 is affected by lag error that was corrected through the procedure proposed by Tomasi et al. [26], while the sensor of RS92 does not need any corrections. Each radiosounding profile was projected by means of linear interpolation onto equally spaced 201-height-level grid starting from the station surface level, having 100 m as the second level and reaching 20 km after that with a step

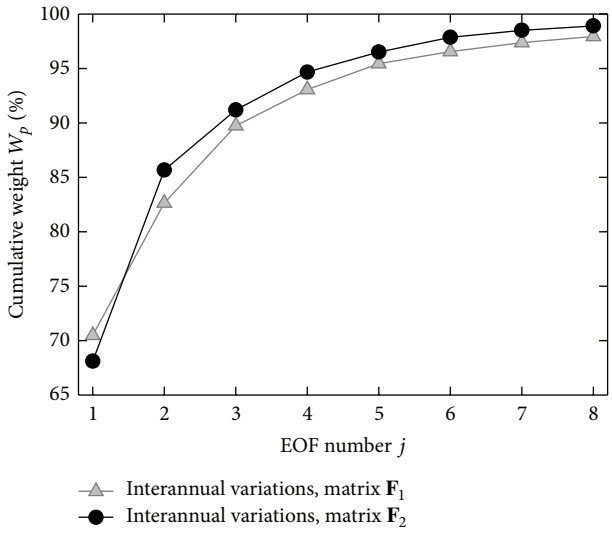

FIGURE 3: Cumulative weight W_p of the EOFs found for both cases of temperature anomalies and subject of the present study.

of 100 m. Figure 1 presents the result of this procedure applied on three temperature profiles observed at the station on different days of the examined period. Further, these profiles formed the matrix $\mathbf{F}'$, in which they were consecutively inserted as rows and the gaps in the columns of $\mathbf{F}'$, resulted from sporadically missing radio sound launches, were filled by means of linear interpolation to obtain sequences with a step of 12 hours. In order to eliminate the oscillations associated with micro- and mesoscales atmospheric processes considered shorter than 10 days [27], sequences, that consisted of 10-day average values of the temperature as illustrated in Figure 2(a) by the red curve, replaced the columns in $\mathbf{F}'$. It is seen from Figure 2(a) that the temperature variations present well marked oscillations with a period close to 1 year modulated by lower frequency fluctuations. Since the amplitude of these two types of oscillations is quite different, it seems reasonable to separate them for the next analysis. For that purpose, a running average procedure with 30-day window was applied to obtain the long-period variations given by the blue curve in Figure 2(a). The difference between sequences represented by the red and blue curves is shown in Figure 2(b) and it is considered to represent the intra-annual temperature oscillations, or the oscillations characterized by periods lower than 1 year that form the anomaly matrix $\mathbf{F}_1$ subject of the further analysis. Time series, presenting the long-period oscillations, were detrended by removing from each of them the corresponding trend, found through linear approximation, and the result is given by the azure curve in Figure 2(c). The spectral analysis showed that these oscillations were strongly dominated by the annual and semiannual cycles that masked the other long-period fluctuations and hence, it was decided to remove them from the data. Such a filtering was performed by extracting the variations that consisted of periods lower than 1 year, which are presented by the brown curve in Figure 2(c), from the long-period temperature oscillations given by the azure curve in the same figure. At the end, Figure 2(d) exhibits the resulting curve that represents the interannual oscillations composing the second anomaly matrix $\mathbf{F}_2$ analysed in the present study.

3. Results and Discussion

The cumulative weight curves of the EOFs obtained for the intra- and interannual temperature variations, presented by matrices $\mathbf{F}_1$ and $\mathbf{F}_2$, respectively, and shown in Figure 3, indicate that in both cases the first four components explain 93–95% of the temperature variations. These EOFs are given in Figure 4, while Figures 5 and 6 exhibit the corresponding PCs on the left-hand side and their spectra on the right. The EOFs represent the vertical profiles of the temperature anomalies that can be considered the amplitude of variations determined by the corresponding PCs, so that each of the two groups containing four EOF-PC pairs defines the corresponding type of temperature variations (intra- or interannual), given by matrices $\mathbf{F}_1$ and $\mathbf{F}_2$.

Figures 5 and 6 reveal that each PC in both cases is characterised by a spectral band dominating on the other frequencies. It can be seen from Figure 5(b) that the leading PC1 of the matrix $\mathbf{F}_1$ consists mainly of periods pertaining to 30–120-day band with peaks at 51, 54, 73, and 98 days that can be associated with the MJO [4] and AO [6, 7] oscillations or with an interaction between them according to the conclusions made by Zhou and Miller [14]. In addition, these oscillations are modulated by the annual cycle that has secondary importance for the PC1 variations. The corresponding EOF1 given in Figure 4(a) shows that PC1 oscillations are presented in the troposphere between 1 and 8 km, while in the tropopause zone the amplitude decreases changing the sign that can be interpreted as changing of the fluctuation phase. In the low stratosphere the PC1 oscillations gradually decrease. It should be pointed out that this EOF1-PC1 pair explains about 70% of the intra-annual temperature variations at the San Pietro Capofiume station.

The second component EOF2 of the anomaly matrix $\mathbf{F}_1$ that contributes to the variations by about 12% is presented in Figure 4(b), while the corresponding PC2 and its spectrum are given in Figures 5(c) and 5(d), respectively. It is seen from Figure 4(b) that these oscillations are uniformly weak in all altitude range with a slight enhancement in the upper troposphere-low stratosphere (UTLS) range. The spectrum shows that the PC2 variations are strongly modulated by the annual and semiannual cycles while the fluctuations with periods of 30–100 days are weaker by approximately an order of magnitude.

Figure 4(c) shows EOF3 component that indicates almost null amplitude of the oscillations in the troposphere and values between −1 and 1 K in UPLS. This component has a low contribution (~7%) with a prevailing weight of the 120-day period in the corresponding PC3 component (Figure 5(e)) as the spectrum given in Figure 5(f) reveals. The EOF4 weight in the temperature oscillations is about 3% and this component presents variations mainly in the 9–15 km altitude range (see Figure 4(d)) that consist of periods between 30 and 120 days with peaks at 52, 62, 72, 82, and 120 days (Figures 5(g) and 5(h)).

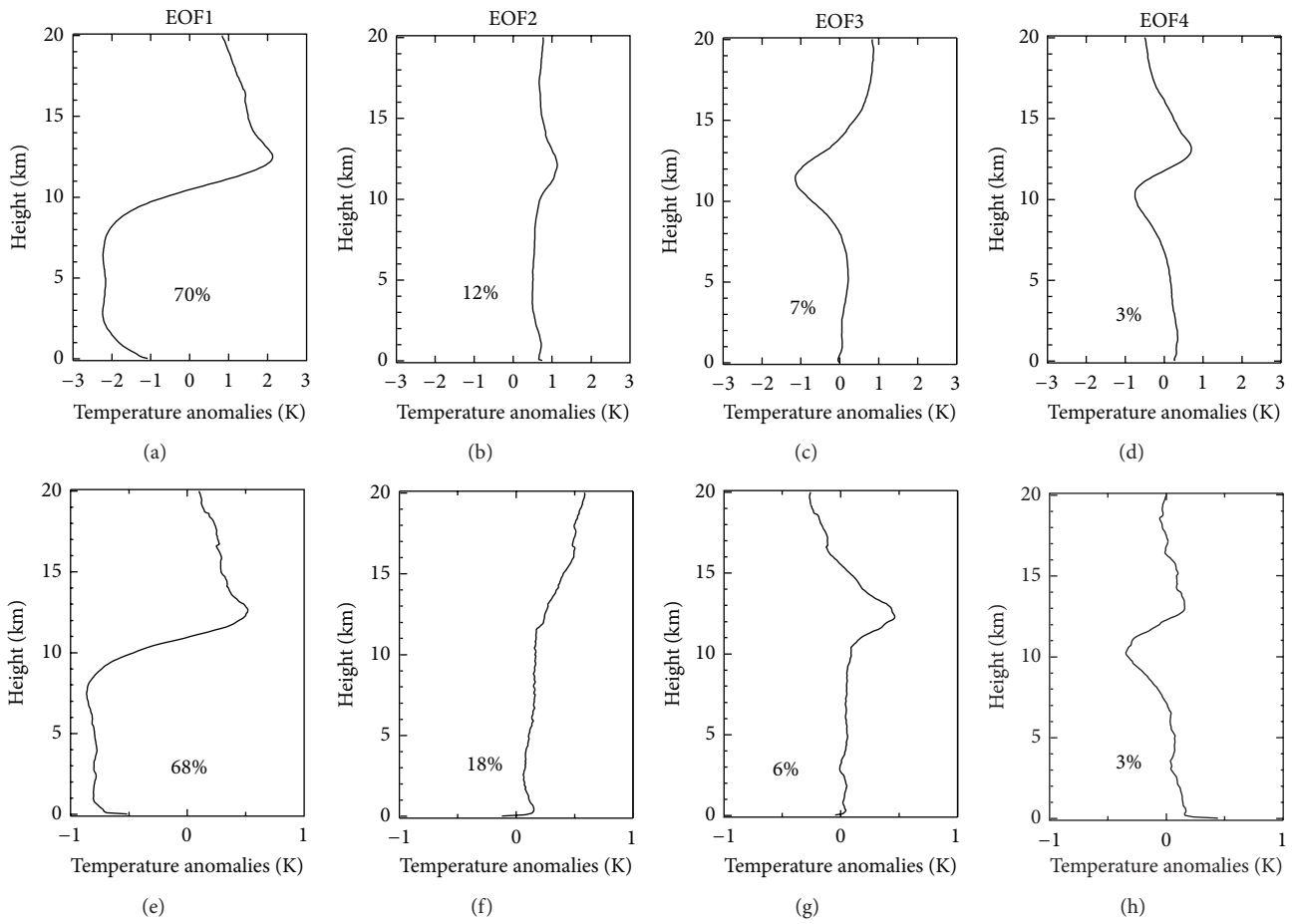

FIGURE 4: The first four EOFs evaluated for the matrix $\mathbf{F}_1$ (intra-annual variations, up) and $\mathbf{F}_2$ (interannual variations, down). The corresponding weight w_j of each component, evaluated through (3), is given in each panel.

Figures 4(e)–4(h) and 6 exhibit the EOFs and PCs, respectively, obtained from decomposition of the matrix $\mathbf{F}_2$, representing the temperature anomalies associated with the interannual oscillations. The first component EOF1 (Figure 4(e)) that contributes to the oscillations by about 68% shows a pattern analogous to the EOF1 of the intra-annual fluctuations (Figure 4(a)), presenting the largest amplitude of about 1 K in the troposphere between 1 and 9 km that rapidly decreases in the region of the tropopause. In the upper-altitude range, the amplitude changes the sign and increases until about 13 km gradually decreasing to zero after that. The corresponding temporal variations presented by PC1, shown in Figure 6(a), are composed of spectral components ranging between 1- and 7-year periods with peaks at 1.3, 1.7, 2.3, 2.9, and 6.8 years, as Figure 6(b) indicates. The period at 2.9 years exhibits the highest spectral power followed by the periods at 1.7 and 6.8 years. The ratio between powers of 2.9- and 6.9-year periods is very similar to that presented by the corresponding components of the ESNO index spectrum given in the Stenseth et al. [10] study (their Figure 2(c)). Such a similarity leads to the assumption that the ENSO are strongly presented in the leading PC of the interannual temperature fluctuations. The other spectral components that present a secondary importance could be associated with the QBO and its interaction with the annual cycle [8]. EOF2, exhibited in Figure 4(f), shows 18% contribution with negligible effect in the troposphere and increasing amplitude in UTLS. The temporal variations associated with this component, presented by PC2 in Figure 6(c), consist predominantly of 21-year cycle that can be linked up with the 22-year solar cycle and a secondary peak at 1.5 years as Figure 6(d) indicates. Similarly to EOF2, EOF3 presents higher contribution in UTLS (see Figure 4(g)) but only about 6% weight in the temperature variations. The oscillations of EOF3 (PC3) given in Figure 6(e) are dominated by 10.3-year cycle with secondary peaks at 1.9-, 2.3-, and 2.9-year fluctuations. The first cycle could be accounted for the 11-year solar cycle, while the others can be interpreted as a manifestation of the QBO and ENSO or NAO fluctuation components. Figure 4(h) shows that EOF4, which contributes to the interannual temperature fluctuations by about 3%, shows significant amplitudes between 8 and 12 km, the region of the tropopause altitudes. The corresponding PC4 given in Figure 6(g) is composed of oscillations characterized by a large band between 4- and 8-year periods and a secondary peak at 1.5-year period. The oscillations pertaining to the first

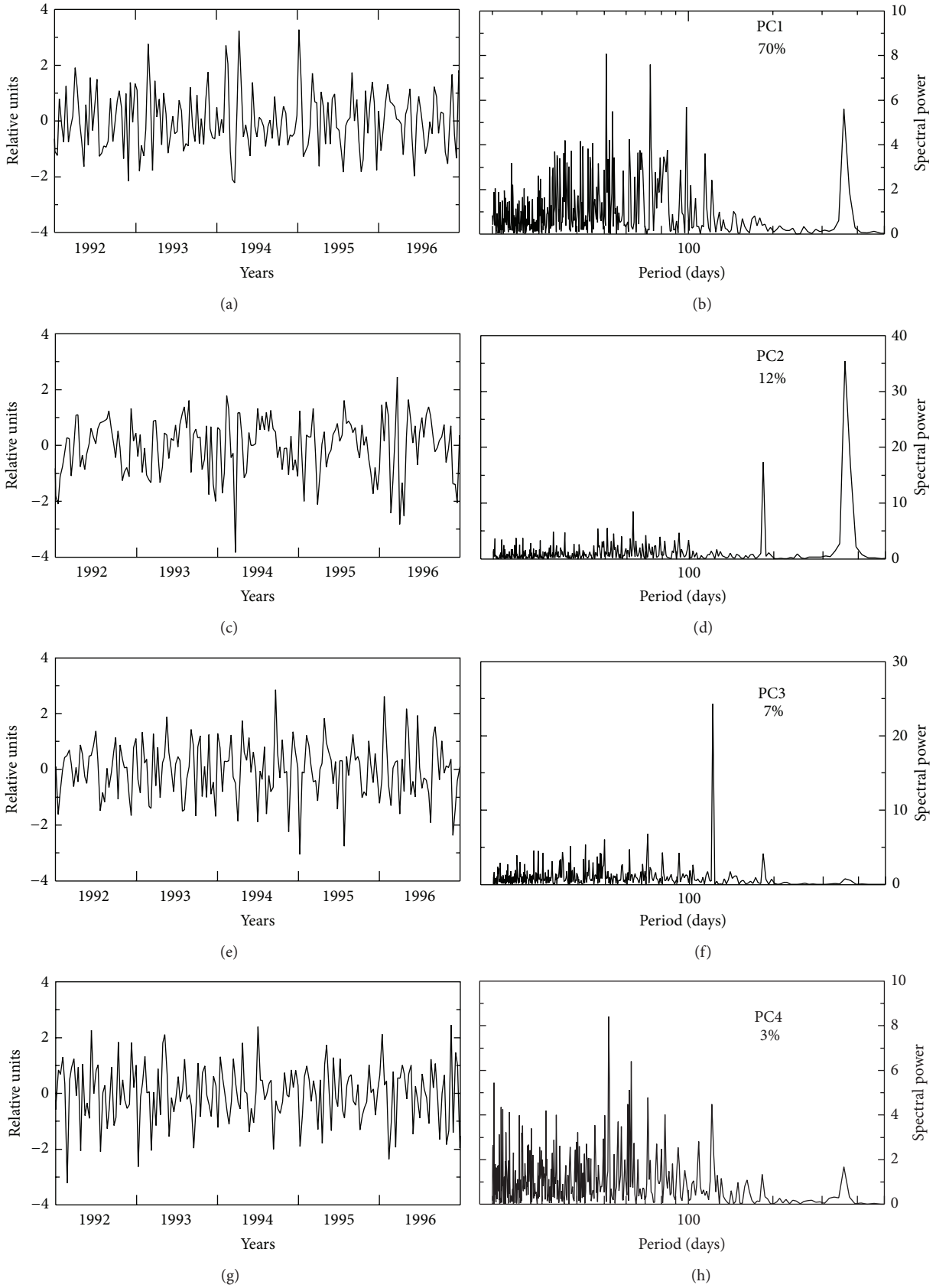

Figure 5: The leading four PCs presented for a 5-year period (left) that are associated with the corresponding EOFs found from the decomposition of matrix $\mathbf{F}_1$ (see upper part of Figure 4) together with their spectra (right). The two panels of each row correspond to the same PC indicated on the right, together with its weight w_j in percent.

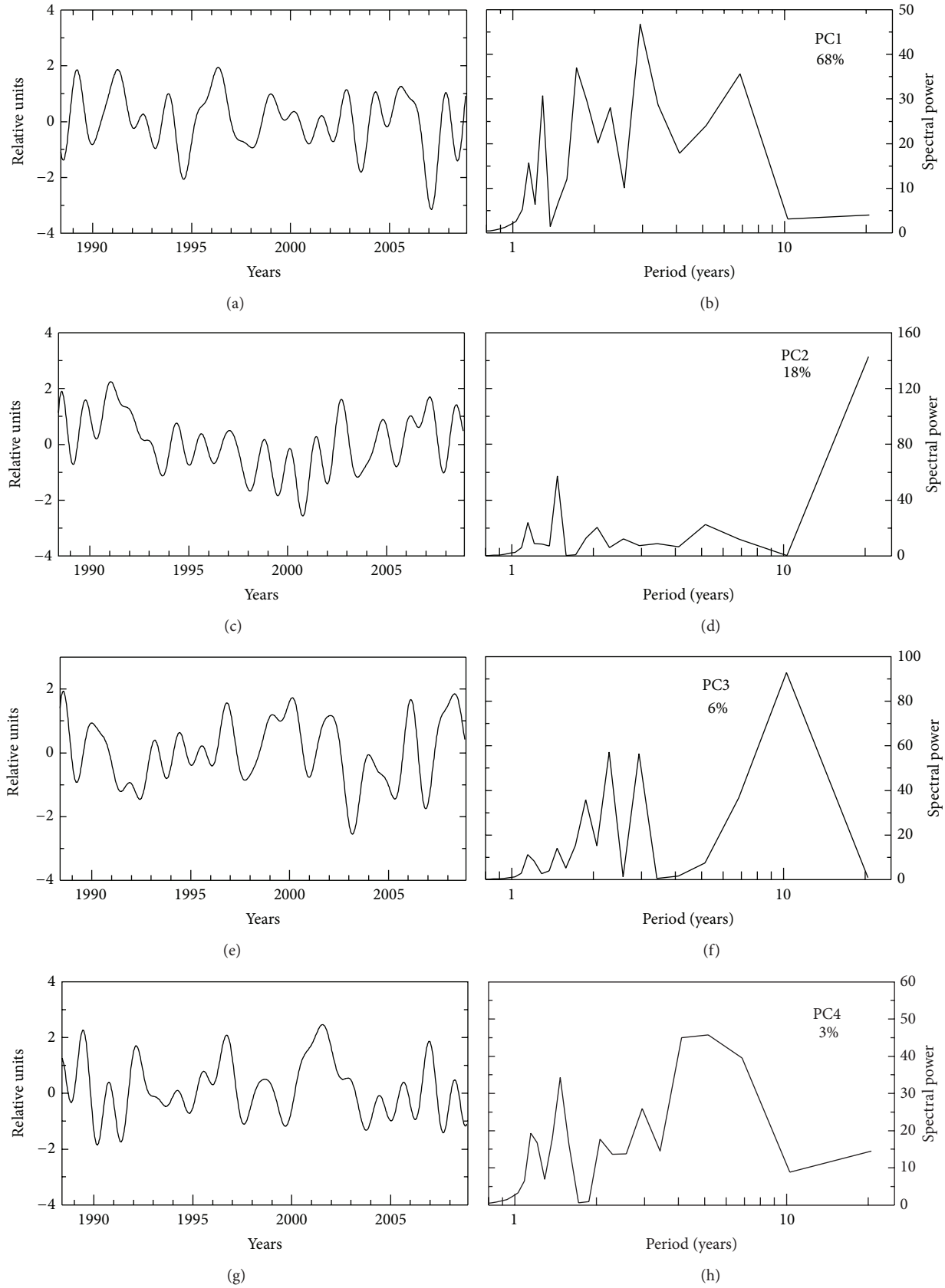

FIGURE 6: PCs of matrix $\mathbf{F}_2$ corresponding to the EOFs of the lower part of Figure 4 are exhibited analogously to the same parameters of the matrix $\mathbf{F}_1$ in Figure 5.

spectral range could be associated with the 6–10-year band of the NAO [12].

It is worth pointing out that all EOFs corresponding to the interannual temperature variations taken place at the station subject of the present study and given in the lower part of Figure 4 exhibit strong amplitude gradients in the boundary layer.

4. Conclusions

The present study has analysed the temperature variations observed above the southeast part of the Po Valley, Italy, up to 20 km by means of radio sounds launched twice a day during about 22-year period. The principle component analysis of the data allowed the projection of the temperature variations over four principle vertical distribution and temporal modes, respectively. Such an analysis shows that except the annual cycle, strongly presented in all altitude levels, the intra-annual oscillations composed of periods between 30 and 120 days, together with the interannual variations with periods of 1 to 7 years, predominantly determine the temperature fluctuations in the troposphere. The first type of oscillations can be associated with MJO and their interaction with AO, while the second group could be accounted for the ESNO and QBO. These variations vanish in the tropopause region and, changing the phase appearance to different extent in the low stratosphere. The annual and semiannual pulsations of the amplitude characterising the short-period mode are of secondary importance and are presented mainly in the 10–13 km range, where the tropopause altitude usually varies, while the oscillations with 120-day period present minor contribution and could be observed in UTLS. The interannual oscillations described by EOF2-4 components that could be associated with global fluctuations as ESNO, QBO, and NAO are negligibly weak in the troposphere and take place mainly in the UTLS region.

Conflict of Interests

The author declares that there is no conflict of interests regarding the publication of this paper.

Acknowledgments

The radio soundings data recorded at the San Pietro Capofiume station located in the southeast part of the Po Valley have been downloaded from the website of the University of Wyoming (http://weather.uwyo.edu/upperair/sounding.html).

References

[1] G. C. Reid, "Seasonal and interannual temperature variations in the tropical stratosphere," *Journal of Geophysical Research*, vol. 99, no. 9, pp. 18923–18932, 1994.

[2] X. Dou, T. Li, J. Xu et al., "Seasonal oscillations of middle atmosphere temperature observed by Rayleigh lidars and their comparisons with TIMED/SABER observations," *Journal of Geophysical Research D: Atmospheres*, vol. 114, no. 20, Article ID D20103, 2009.

[3] I. Isaia, "Oscillations and cycles of air temperature in Russia," *Present Environment and Sustainable Development*, vol. 8, no. 1, pp. 191–203, 2014.

[4] R. A. Madden and P. R. Julian, "Detection of a 40–50 day oscillation in the zonal wind in the tropical Pacific," *Journal of the Atmospheric Sciences*, vol. 28, no. 5, pp. 702–708, 1971.

[5] C. Zhang, "Madden-julian oscillation," *Reviews of Geophysics*, vol. 43, no. 2, Article ID RG2003, pp. 1–36, 2005.

[6] D. W. J. Thompson and J. M. Wallace, "The Arctic oscillation signature in the wintertime geopotential height and temperature fields," *Geophysical Research Letters*, vol. 25, no. 9, pp. 1297–1300, 1998.

[7] M. P. Baldwin and T. J. Dunkerton, "Propagation of the Arctic Oscillation from the stratosphere to the troposphere," *Journal of Geophysical Research D: Atmospheres*, vol. 104, no. 24, pp. 30937–30946, 1999.

[8] M. P. Baldwin, L. J. Gray, T. J. Dunkerton et al., "The quasi-biennial oscillation," *Reviews of Geophysics*, vol. 39, no. 2, pp. 179–229, 2001.

[9] C. Wang, C. Deser, J.-Y. Yu, P. DiNezio, and A. Clement, "El Niño and southern oscillation (ENSO): a review," in *Coral Reefs of the Eastern Pacific*, pp. 3–19, 2012.

[10] N. C. Stenseth, G. Ottersen, J. W. Hurrell et al., "Studying climate effects on ecology through the use of climate indices: the North Atlantic Oscillation, El Niño Southern Oscillation and beyond (Review)," *Proceedings of the Royal Society of London B*, vol. 270, no. 1529, pp. 2087–2096, 2003.

[11] R. García-Herrera, N. Calvo, R. R. Garcia, and M. A. Giorgetta, "Propagation of ENSO temperature signals into the middle atmosphere: a comparison of two general circulation models and ERA-40 reanalysis data," *Journal of Geophysical Research*, vol. 111, no. 6, Article ID D06101, 2006.

[12] H. Wanner, S. Brönnimann, C. Casty et al., "North Atlantic oscillation—concepts and studies," *Surveys in Geophysics*, vol. 22, no. 4, pp. 321–382, 2001.

[13] N.-C. Lau, "Interactions between global SST anomalies and the midlatitude atmospheric circulation," *Bulletin of the American Meteorological Society*, vol. 78, no. 1, pp. 21–33, 1997.

[14] S. Zhou and A. J. Miller, "The interaction of the Madden-Julian oscillation and the Arctic oscillation," *Journal of Climate*, vol. 18, no. 1, pp. 143–159, 2005.

[15] M. F. Stuecker, A. Timmermann, F.-F. Jin, S. McGregor, and H.-L. Ren, "A combination mode of the annual cycle and the El Niño/Southern Oscillation," *Nature Geoscience*, vol. 6, no. 7, pp. 540–544, 2013.

[16] B. Dewitte, C. Cibot, C. Périgaud, S.-I. An, and L. Terray, "Interaction between near-annual and ENSO modes in a CGCM simulation: role of the equatorial background mean state," *Journal of Climate*, vol. 20, no. 6, pp. 1035–1052, 2007.

[17] X. Zheng and R. E. Basher, "Structural time series models and trend detection in global and regional temperature series," *Journal of Climate*, vol. 12, no. 8, pp. 2347–2358, 1999.

[18] A. J. Simmons, K. M. Willett, P. D. Jones, P. W. Thorne, and D. P. Dee, "Low-frequency variations in surface atmospheric humidity, temperature, and precipitation: inferences from reanalyses and monthly gridded observational data sets," *Journal of Geophysical Research D: Atmospheres*, vol. 115, no. 1, Article ID D01110, 2010.

[19] D. T. Mihailović, G. Mimić, and I. Arsenić, "Climate predictions: the chaos and complexity in climate models," *Advances in Meteorology*, vol. 2014, Article ID 878249, 14 pages, 2014.

[20] S. A. Solman, "Regional climate modeling over south america: a review," *Advances in Meteorology*, vol. 2013, Article ID 504357, 13 pages, 2013.

[21] H. Björnsson and S. A. Venegas, "A manual for EOF and SVD analyses of climatic data," Tech. Rep. 97-1, McGill University, Montreal, Canada, 1997.

[22] A. Hannachi, I. T. Jolliffe, and D. B. Stephenson, "Empirical orthogonal functions and related techniques in atmospheric science: a review," *International Journal of Climatology*, vol. 27, no. 9, pp. 1119–1152, 2007.

[23] C. D. Camp, M. S. Roulston, and Y. L. Yung, "Temporal and spatial patterns of the interannual variability of total ozone in the tropics," *Journal of Geophysical Research*, vol. 108, no. 20, article 4643, 2003.

[24] N. R. Lomb, "Least-squares frequency analysis of unequally spaced data," *Astrophysics and Space Science*, vol. 39, no. 2, pp. 447–462, 1976.

[25] J. D. Scargle, "Studies in astronomical time series analysis. II—statistical aspects of spectral analysis of unevenly spaced data," *The Astrophysical Journal*, vol. 263, pp. 835–853, 1982.

[26] C. Tomasi, B. Petkov, E. Benedetti et al., "Characterization of the atmospheric temperature and moisture conditions above Dome C (Antarctica) during austral summer and fall months," *Journal of Geophysical Research*, vol. 111, no. 20, Article ID D20305, 2006.

[27] D. G. Steyn, T. R. Oke, J. E. Hay, and J. L. Knox, "On scales in meteorology and climatology," *Climate Bulletin*, vol. 39, pp. 1–8, 1981.